COMPARISON OF HIGH-n INSTABILITIES INCLUDING ALPHA-PARTICLE EFFECTS IN BPX AND TFTR

PPPL--2772

DE91 015375

G. REWOLDT

Plasma Physics Laboratory, Princeton University,

Princeton, New Jersey

United States of America

ABSTRACT. Three distinct types of high toroidal mode number instabilities are obtained from a comprehensive kinetic calculation, using as input transport code results from the analysis of a recent design for the Burning Plasma Experiment (BPX). These instabilities are: the collisionless trapped-electron ion-temperature-gradient mode, the magnetohydrodynamic ballooning mode, and a high toroidal mode number version of the toroidicity-induced Alfvén eigenmode or "gap" mode. The dependence of the instability linear eigenfrequencies on minor radius, beta, and toroidal mode number are investigated, along with the effects of hot alpha particles. Relative quasilinear fluxes of particles and energy for each species are also obtained. In addition, the beta dependence of the magnetohydrodynamic ballooning mode is investigated for a case using as input the results of a transport code calculation for the Tokamak Fusion Test Reactor (TFTR) in an extrapolation to a deuterium-tritium mixture. The effects of alpha particles and the relative quasilinear fluxes are also investigated for this case.

1. INTRODUCTION

A comprehensive toroidal kinetic analysis for high-n (toroidal mode number) instabilities has been described in detail in Refs. [1] and [2]. The associated computer code has been applied to the study of alpha-particle effects on the trapped-electron drift mode and the magnetohydrodynamic (MHD) ballooning mode in Ref. [3] for cases corresponding to an earlier design of the Burning Plasma Experiment (BPX), then called the Compact Ignition Tokamak (CIT), and to the Tokamak Fusion Test Reactor (TFTR). In the present work, an additional instability is studied, namely the high-n version of the so-called "toroidicity-induced Alfvén eigenmode" (TAE) or "gap" mode, previously studied for low n in Ref. [4] and, in a less comprehensive calculation than the present one, for high n in Ref. [5]. Alpha particle effects on the low-n TAE mode have been investigated in Ref. [6]. The potential relevance of this type of instability has gained support from recent experimental results indicating their possible presence[7].

In discussing the properties of the TAE mode, it is convenient to refer to it as the ω_A root, because the real frequency ω_r is of the order of the Alfvén frequency $\omega_A \equiv v_A/qR_0$, where $v_A \equiv B_0/(4\pi n_i m_i)^{1/2}$ is the Alfvén velocity. Also, the MHD ballooning mode will be referred to as the ω_{*pi} root, because, when kinetic effects are included, its real frequency ω_r is of the order of ω_{*pi}, the ion diamagnetic frequency determined by the ion pressure gradient. Toroidal electrostatic drift modes are destabilized by the combined effects of the unfavorable trapped-electron time-average magnetic drift (precession) frequency, responsible for driving the collisionless trapped-electron mode, and by the familiar ion temperature gradient [$\eta_i \equiv (d\ln T_i/dr)/(d\ln n_i/dr)$] mechanism, as pointed out in Ref. [8]. Accordingly, this type of instability is referred to as the trapped-electron-η_i mode.

The first of the specific cases investigated here employs the output from a run[9] of the BALDUR transport code[10] for a recent design of BPX with major radius $R_0 = 2.6$ m, magnetic field on axis $B_0 = 9.0$ T, and plasma current $I_p = 11.8$ MA. Results are also presented here for a case corresponding to an extrapolation[11] for TFTR to an equal

mixture of deuterium and tritium, from a previous deuterium-only experimental discharge, with moderately optimistic assumptions yielding $Q \equiv$ fusion power / external heating power $= 0.5$.

The linear and quasilinear calculation employed here can be either electrostatic or fully electromagnetic, and it includes all of the relevant kinetic effects for the magnetically trapped and untrapped particles of each species. These effects include bounce frequency resonances for trapped particles, transit frequency resonances for untrapped particles, and magnetic curvature and gradient drift frequency effects, without any ordering between these frequencies and the mode frequency. Full finite Larmor radius effects are included. The analysis makes use of the so-called "ballooning formalism" at lowest order[12], which yields a radially local calculation for the eigenfrequency and eigenfunction. The so-called "$1/n$" correction term at higher order[12] can also be included.

The input data for the calculation can be obtained from running the BALDUR transport code or another transport code, or from experimental data. This information includes the safety factor $q(r)$, the densities $n_j(r)$, and the temperatures $T_j(r)$, for $j = e$, i, α, where e refers to electrons, i refers to a single ionic species of mass 2.5 amu representing an equal mixture of deuterium and tritium, and α refers to the hot alpha particles. The equilibrium distribution functions for the electrons and ions, the background species, are taken to be Maxwellian, which is a good approximation, and that for the alphas is taken to be a "slowing-down" distribution, $F_\alpha = F_{SD} \propto (v^3 + v_c^3)^{-1}$, where v_c is the so-called critical velocity. This should be an adequate approximation for the hot alphas, and the sensitivity to this choice is investigated in Ref. [3] where results with a slowing-down distribution and with a Maxwellian distribution for the alphas are compared. Using the safety factor and pressure profiles from the transport code calculation, the MHD equilibrium is obtained numerically. In this process, the density profiles $n_j(r)$, and thus $p(r)$ and $\beta(r)$, can be multiplied by a constant and the MHD equilibrium numerically recomputed. This allows artificial variation of $\beta \propto n_j$ at fixed T_j and B_0. Note that, with this prescription, the Alfvén velocity $v_A \equiv B_0/(4\pi n_i m_i)^{1/2}$ and

the Alfvén frequency $\omega_A \equiv v_A/qR_0$ both vary as $\beta^{-1/2}$. In addition, $k_\theta \rho_i \propto n$ is varied to find the maximum of the linear growth rate γ, and r is varied to explore the radial dependence of the eigenfrequency, for each of the three types of instabilities considered.

The effect of the hot alpha particles can be isolated by turning their number density fraction, n_α/n_e, on or off, at fixed $n_e(r)$. In order to preserve the condition of local equilibrium charge neutrality, $\sum_j n_j e_j = 0$, and its radial derivative, the ion number density fraction, n_i/n_e, and r_{ni}/r_{ne}, where $r_{nj} \equiv -(d \ln n_j/dr)^{-1}$, are adjusted to compensate for the absence of the alphas. Also, the nonadiabatic contributions of the trapped and untrapped alphas can be turned on and off separately, to assess their individual effects.

The calculation also produces the quasilinear particle and energy fluxes for each species for each of the instabilities considered. The *absolute* levels are not directly obtained, because they involve the saturation level ϕ_0 of the perturbed electrostatic potential, which is not determined in a purely linear and quasilinear calculation. However, the *relative* transport for the different species and for particles and energy can be determined for each of the instabilities studies here.

Results are presented in Section 2 for the BPX case for the three types of instabilities, with the r variation considered in Section 2.1, the $\beta \propto n_j$ variation and the hot alpha particle effects in Section 2.2, the $k_\theta \rho_i \propto n$ variation in Section 2.3, the quasilinear transport in Section 2.4, and the $1/n$ correction in Section 2.5. The TFTR case is presented in Section 3. Conclusions are given in Section 4.

2. BPX CASE

Results are presented in this section for the BPX case mentioned in Section 1. The equilibrium profiles for $n_j(r)$, $T_j(r)$, and $q(r)$ are taken from a BALDUR transport code run[9] for a recent design for BPX, at a time in the discharge near the beginning of the flattop period, between sawtooth crashes. The corresponding fixed-boundary MHD equilibrium is computed numerically. The parameters are: major radius $R_0 = 2.6$ m, magnetic field on axis

$B_0 = 9.0$ T, plasma current $I_p = 11.8$ MA, horizontal minor radius $a = 0.8$ m, elongation at boundary = 2.0, triangularity at boundary = +0.35, $q(0) = 0.6745$, $q(a) = 3.309$, $T_e(0) = 18.76$ keV, $T_i(0) = 17.63$ keV, $n_e(0) = 5.238 \times 10^{14}$ cm^{-3}, $\beta(0) = 9.48\%$ without alpha particles, $\beta(0) = 11.1\%$ with alpha particles, and $n_\alpha(0)/n_e(0) = 0.006751$. The electron density profile $n_e(r)$ is very flat in the interior, comparable to an H-mode discharge. The hot alpha particle density profile $n_\alpha(r)$ is strongly localized about $r = 0$. The electron and ion temperature profiles are normally peaked. Also, as is normal with a "slowing-down" distribution function, the radial profile of the effective temperature for the hot alphas is quite flat, and the hot alpha particle temperature gradient is neglected here.

2.1. Radial dependence

The radial dependence of the linear growth rates γ for the three types of instabilities is displayed in Fig. 1, and the corresponding real frequencies ω_r are displayed in Fig. 2. In these two figures, the eigenfrequencies for the trapped-electron-η_i mode and the ω_{*pi} root are shown for the case with alpha particles replaced by background ions, because alphas are not necessary to cause instability for these two roots. However, for the ω_A root, the eigenfrequencies are shown including the hot alpha particles, because they are needed for instability for that root. The effects of alpha particles will be discussed in more detail in Section 2.2. Also, in Figs. 1 and 2, the values of $\beta(r)$ used for the trapped-electron-η_i mode are those calculated directly from the BALDUR values of $n_j(r)$ and $T_j(r)$, since this mode is unstable for these β values. However, for the ω_{*pi} root and the ω_A root, the values of $\beta(r)$ have been doubled by doubling $n_j(r)$ for all species, because the critical β values for instability for both of these roots are above the original BALDUR beta values. This β dependence is discussed further in Section 2.2. Collisions are omitted for all three of these roots, since they would have only a very small effect for the present parameters. For instance, even at $r = 75$ cm, where $\nu_e^* \equiv$ effective trapped-electron collision frequency / average trapped-electron bounce frequency = 0.066, the eigenfrequency for the trapped-electron-η_i mode is

$\omega = (-0.80 + 3.84i) \times 10^5$ sec^{-1} without collisions and $\omega = (-0.95 + 3.57i) \times 10^5$ sec^{-1} with collisions, a difference of only 7% in the growth rates. For smaller r, the difference would would be even smaller because of the higher T_j. For the ω_{*pi} root, the effect of collisions is even weaker, as is discussed in Ref. [2].

The MHD equilibrium employed here contains finite-β effects such as the Shafranov shift, with the consequent reduction in the amount of "bad" curvature. The calculations of the eigenfrequencies for the ω_{*pi} root and the ω_A root are fully electromagnetic, including $\tilde{\Phi}$, $\tilde{A}_{\|}$, and $\tilde{A}_{\perp}$. However, the results shown in Figs. 1 and 2 for the trapped-electron-η_i mode are obtained in the electrostatic limit, retaining only $\tilde{\Phi}$ in the calculation. Again, this is done because electromagnetic effects are rather weak for this mode in this case; at $r = 39$ cm without alpha particles, $\omega = (-1.28 + 0.40i) \times 10^5$ sec^{-1} in the electrostatic limit, and $\omega = (-1.22 + 0.51i) \times 10^5$ sec^{-1} in the full electromagnetic calculation. For the present survey of the radial dependence of the eigenfrequency of the trapped-electron-η_i mode, the electrostatic approximation is sufficiently accurate and requires much less computer time.

As can be seen in Fig. 1, the growth rates for the ω_{*pi} root and the ω_A root peak radially near the center of the discharge, inside the $q = 1$ surface, where the pressure gradients are largest. Also, the ω_A root is destabilized by the hot alpha particles and their density gradient is largest near the magnetic axis. The trapped-electron-η_i mode growth rate, on the other hand, increases rather strongly out to the plasma boundary at $a = 80$ cm in this case which has only a very small background density gradient in the interior. Since $\eta_i \equiv (d \ln T_i/dr)/(d \ln n_i/dr) \gg 1$ at all radii in this case, the characteristics of this root are those of the ion temperature gradient (η_i) mode.

The associated real frequencies ω_r are shown in Fig. 2. They are all in the ion diamagnetic direction; this is normally always the case for the ω_{*pi} root (the MHD ballooning mode) with the inclusion of diamagnetic or finite Larmor radius (FLR) effects, and is expected for the trapped-electron-η_i mode for the present large η_i values. The real frequency for the ω_A root is many times larger than that for the ω_{*pi} root, so they are well separated.

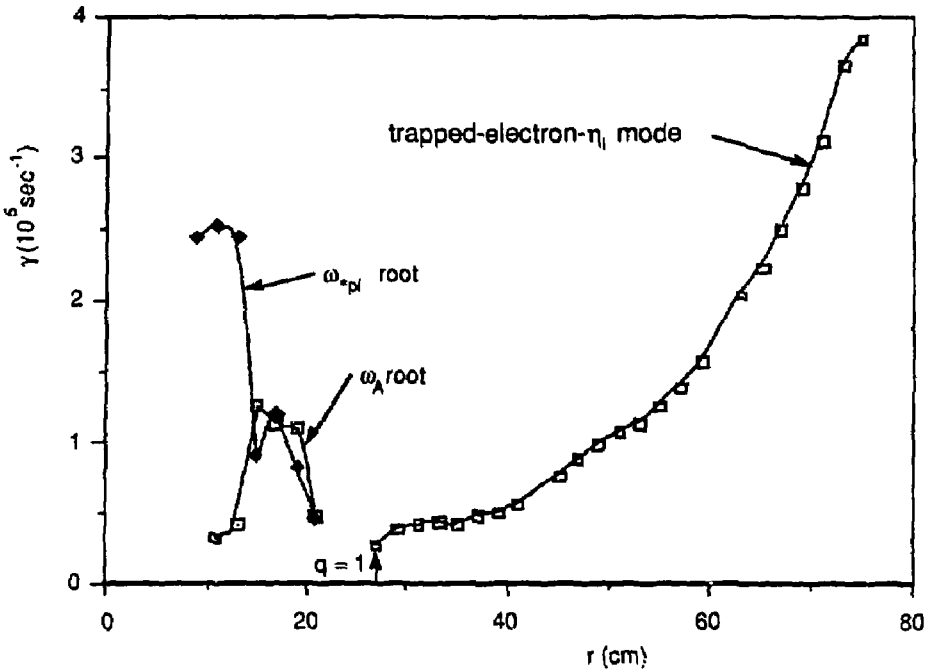

FIG. 1. Radial dependence of the linear growth rates for the BPX case for the ω_{*pi} root (the MHD ballooning mode) with $k_\theta \rho_i \simeq 0.12$, the ω_A root (the TAE or "gap" mode) with $k_\theta \rho_i \simeq 0.086$, and the trapped-electron-η_i mode (the trapped electron drift mode) with $k_\theta \rho_i \simeq 0.34$. The first two roots only have $\beta \propto n_j$ doubled from the BALDUR calculated values. The ω_A root only includes hot alpha particles. The calculations for the first two roots are fully electromagnetic, while that for the trapped-electron-η_i mode is in the electrostatic limit.

2.2. Beta dependence and alpha particle effects

The dependence of the instability growth rates and real frequencies on (toroidal) beta is explored here by multiplying $n_j(r)$ by a single constant for all species j, at fixed $T_j(r)$ and B_0. This is an arbitrary choice, since $T_j(r)$ or B_0 could also be varied, but it has the advantage of

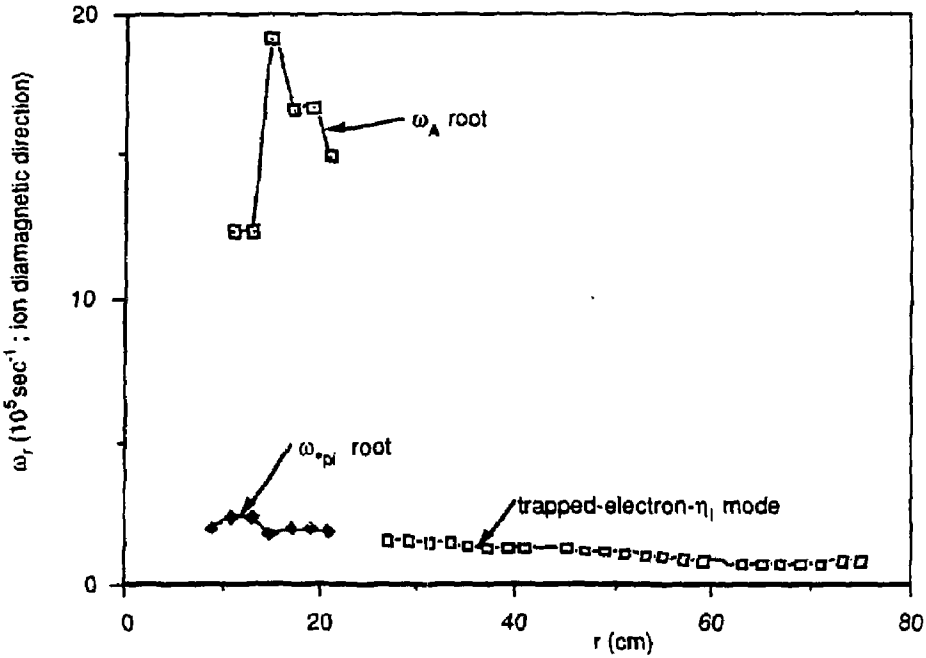

FIG. 2. Real frequencies corresponding to Fig. 1.

varying $v_A \equiv B_0/(4\pi n_i m_i)^{1/2}$ and $\omega_A \equiv v_A/qR_0$ in a simple way, so that the dependences of ω_r on ω_A can be seen. For each new $n_j(r)$, the MHD equilibrium is numerically recomputed, so that the changes in $\beta(r)$, with the corresponding changes in the Shafranov shift and the amount of "bad" curvature, are included.

Figure 3 shows the linear growth rate for the ω_{*pi} root (the MHD ballooning mode) as a function of the local toroidal $\beta \propto n_j$ with hot alpha particles and with the alpha particles replaced by background ions. Results are shown at $r = 11$ cm, where the growth rate has a maximum, for $n \simeq 12$ or $k_\theta \rho_i \simeq 0.12$ or $k_\theta \rho_\alpha \simeq 0.56$, which also maximizes the growth rate. Also shown for reference in Fig. 3 are the results of the simplest ideal MHD ballooning mode equation, without alpha particles or diamagnetic or FLR effects, showing the usual first stability region for $\beta < \beta_{c1} \simeq 13\%$ and the usual unstable region for $\beta > \beta_{c1}$. It is seen

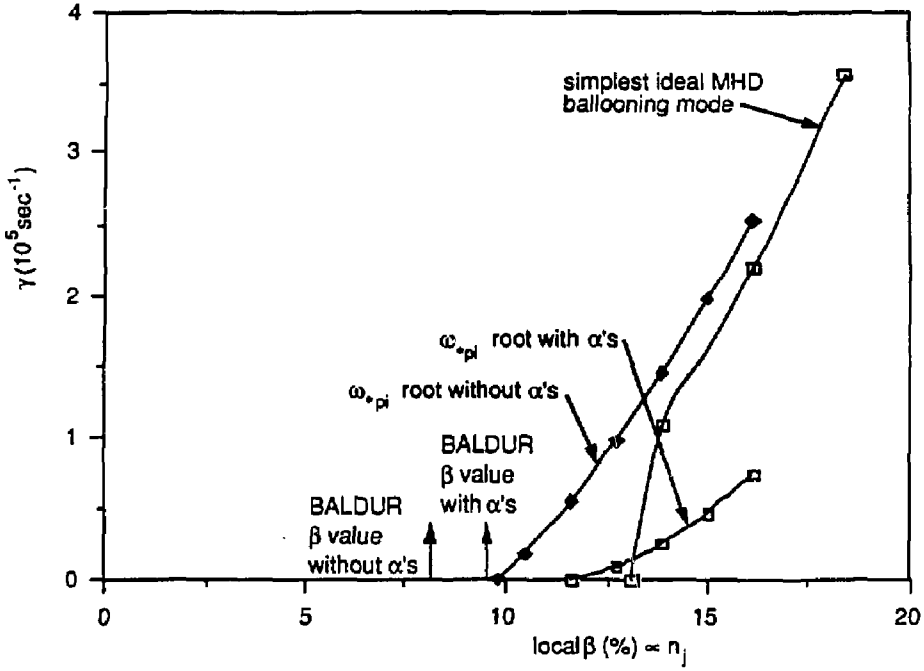

FIG. 3. Growth rate for the ω_{*pi} root as a function of local toroidal β, with and without hot alpha particles for $n = 12$, $k_\theta \rho_i \simeq 0.12$ $k_\theta \rho_\alpha \simeq 0.56$, and $r = 11$ cm. The results of solving the simplest ideal MHD ballooning mode equation, without diamagnetic or FLR effects and without alpha particles, is shown for reference. Here, β is varied by muttiplying $n_j(r)$ by a constant, at fixed $T_j(r)$ and B_0.

that the addition of the kinetic effects for the ω_{*pi} root without alphas has the effect of raising the growth rate slightly in the unstable region, and also of lowering the critical β below β_{c1}, for this particular case and toroidal mode number. However, the addition of the hot alpha particles is stabilizing for this root, and moves the critical β back closer to β_{c1}. For this ω_{*pi} root, the direct effect of the magnetically trapped alpha particles is slightly stabilizing, and that of the untrapped alphas is moderately destabilizing, but the main stabilizing effect

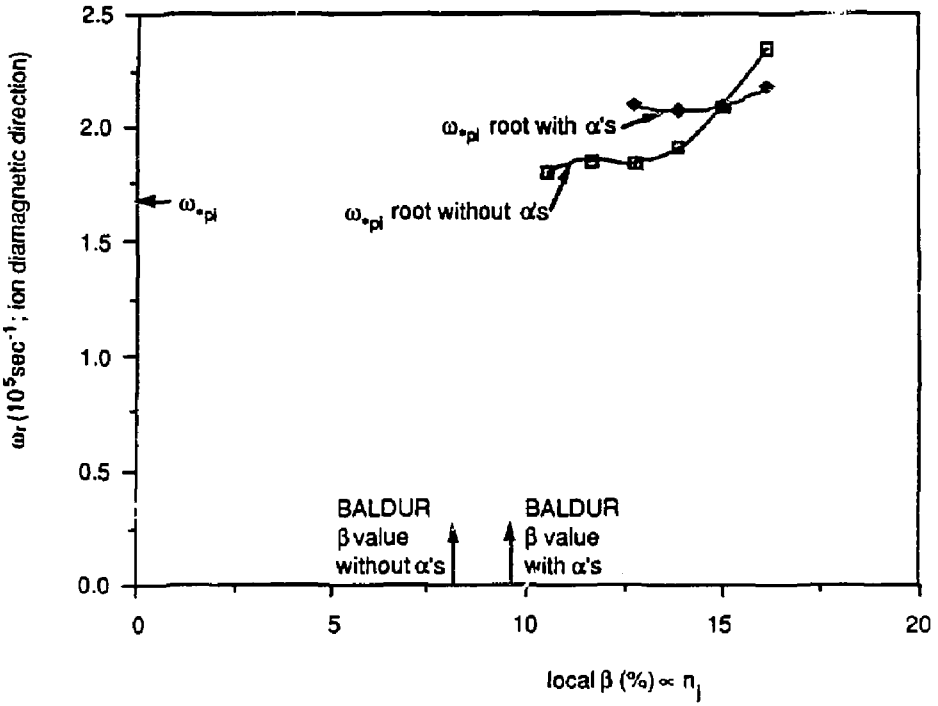

FIG. 4. Real frequencies corresponding to Fig. 3. The real frequency for the simplest ideal MHD ballooning mode is just zero.

comes from the flattening of the background ion density profile necessary to preserve the condition of the radial derivative of equilibrium charge neutrality, with the inclusion of the very steep density profile of the hot alpha particles. The BALDUR calculated β values either with or without alphas are seen to be below the critical β values for this root.

The corresponding real frequencies ω_r for the ω_{*pi} root with and without alphas are shown in Fig. 4. (The real frequency for the simplest ideal MHD ballooning mode without diamagnetic or FLR effects is just zero.) It is seen that ω_r is of the order of $\omega_{*pi} \ll \omega_A$ both with and without alphas, hence the name for this root.

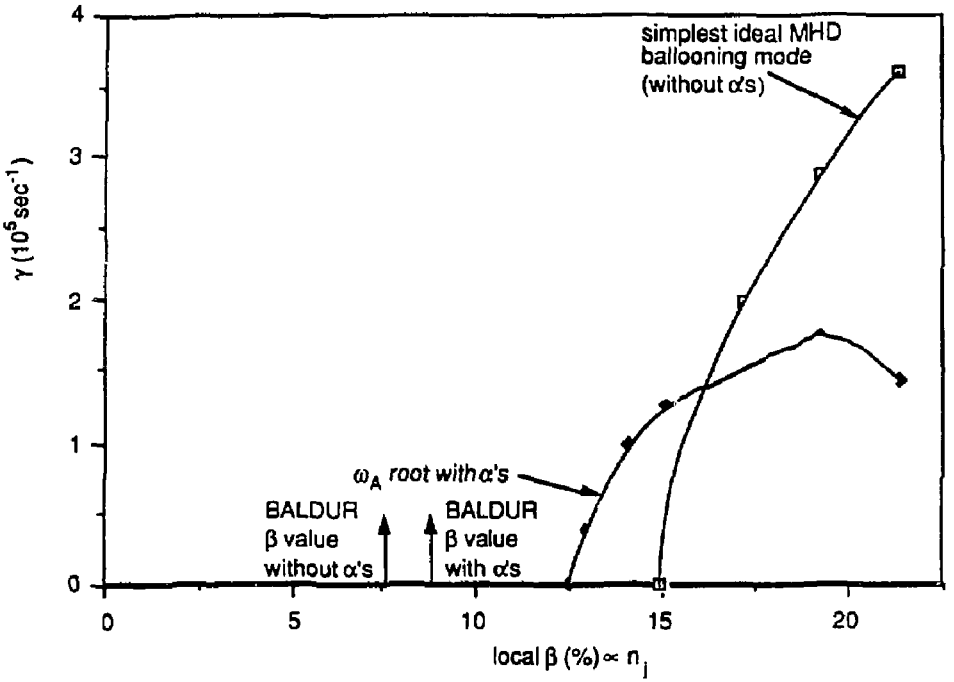

FIG. 5. Growth rate for the ω_A root as a function of the local toroidal β, as in Fig. 3, with hot alpha particles only, for $n = 11$, $k_\theta \rho_i \simeq 0.086$, and $k_\theta \rho_\alpha \simeq 0.41$, at $r = 15$ cm.

For the present case of interest, the growth rates for the ω_A root (the TAE or "gap" mode) are shown in Fig. 5 versus the local toroidal β, for $r = 15$ cm and $n \simeq 11$ or $k_\theta \rho_i \simeq 0.086$ or $k_\theta \rho_\alpha \simeq 0.41$, the values that maximize the growth rate for the mode. Again, the simplest ideal MHD ballooning mode result is shown for reference. Here, the growth rate is shown for the ω_A root only with the hot alpha particles; without the alphas the mode is damped at all β values in this case. The direct destabilization is strong for this root from both the trapped and untrapped alphas, with that from the untrapped alphas being slightly stronger. The critical β for this root is somewhat below the β_{c1} value at this radius. Again,

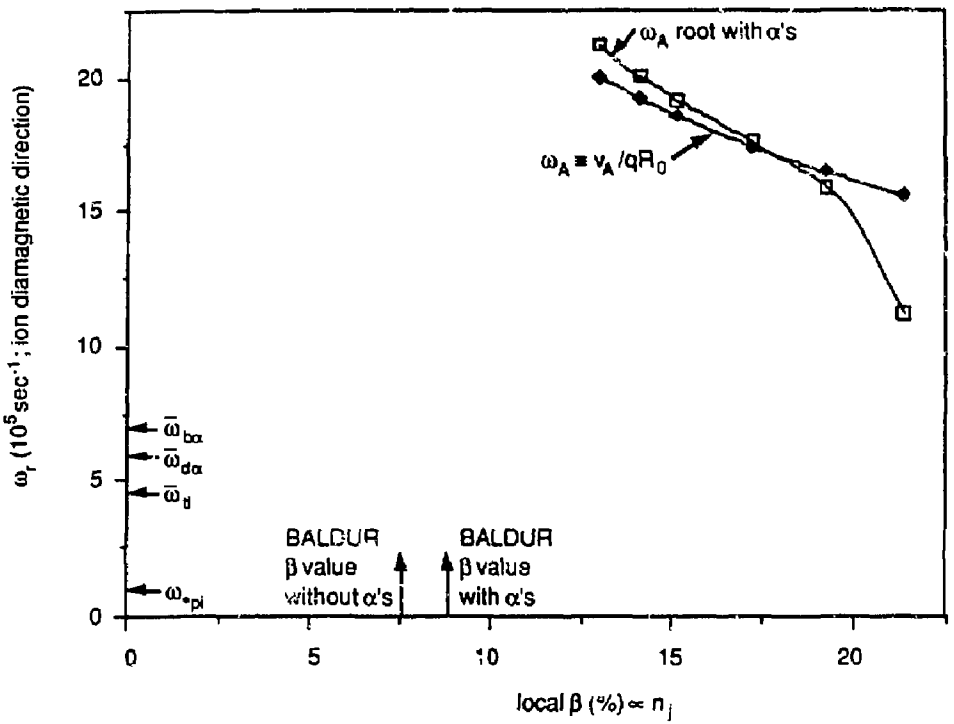

FIG. 6. Real frequencies corresponding to Fig. 5.

the BALDUR calculated β values with or without alphas are below the critical β value for this root.

The corresponding real frequency ω_r for the ω_A root is shown in Fig. 6. Also shown for comparison is the curve for $\omega_A \equiv v_A/qR_0 \propto n_i^{-1/2} \propto \beta^{-1/2}$. It is seen that ω_r for the ω_A root is of the order of $\omega_A \gg \omega_{*pi}$, and tracks roughly along with ω_A except at the highest β point, hence the name for this root. Also, ω_r for the ω_A root is between $\bar{\omega}_{b\alpha}$, the average trapped alpha bounce frequency, and $\bar{\omega}_{t\alpha}$, the average untrapped alpha transit frequency ($\bar{\omega}_{t\alpha} \simeq 30 \times 10^5$ sec^{-1} is slightly offscale on this figure).

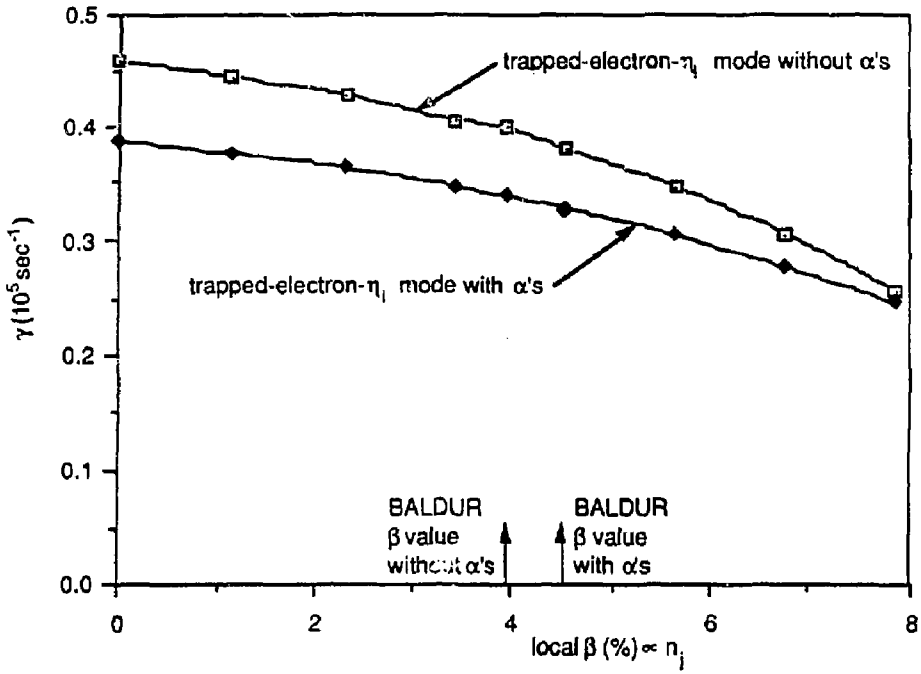

FIG. 7. Growth rate for the trapped-electron-η_i mode as a function of the local toroidal β, in a fully electromagnetic calculation, with and without hot alpha particles, as in Fig. 3, for $n = 114$, $k_\theta \rho_i \simeq 0.34$, and $k_\perp \rho_\alpha \simeq 2.0$, at $r = 39$ cm.

A point to note here is that ω_r for the ω_A root is of order ω_A, not $\omega_A/2 = v_A/2qR_0$ as was found in the original analysis of TAE modes in Refs. [4] and [5] for circular-cross-section cases, (i.e., with ellipticity = 1 on every flux surface). The result that $\omega_r \simeq \omega_A$ here appears to come from the larger ellipticity in the present case (=2.0 at the plasma boundary), which introduces substantial $\cos(2\theta)$ components to the metric quantities describing the numerically calculated MHD equilibrium, and in particular to the quantity $k_\perp$, the wave number magnitude perpendicular to the equilibrium magnetic field line. Here, θ is the poloidal angle variable for the present MHD equilibrium. This effect is seen explicitly in

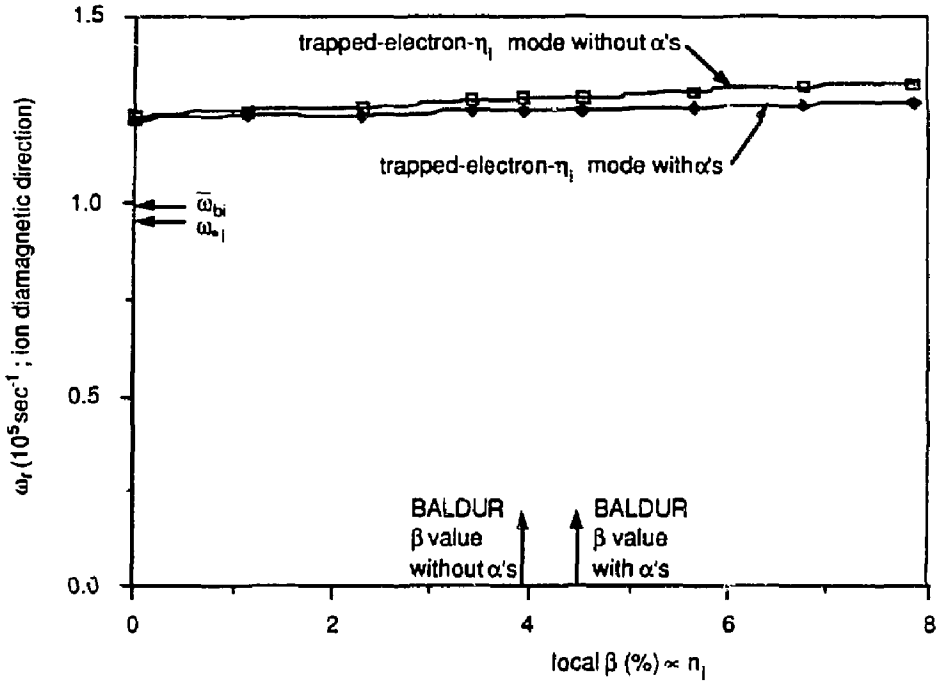

FIG. 8. Real frequencies corresponding to Fig. 7.

Ref. [13], which analyzes low-n "gap" modes in the ideal MHD limit, for cases with small ellipticity and even smaller toroidicity. The low-n "ellipticity induced Alfvén eigenmodes" found in Ref. [13] also have $\omega_r \simeq \omega_A$, not $\omega_A/2$.

The variation of the linear growth rate with $\beta \propto n_j$ for the trapped-electron-η_i mode (which is essentially the η_i or ion temperature gradient mode for the current value of $\eta_i = 3.7$ without alphas) is shown in Fig. 7 for $r = 39$ cm and $n \simeq 114$ or $k_\theta \rho_i \simeq 0.34$ or $k_\theta \rho_\alpha \simeq 2.0$. Now the calculation for this root also is fully electromagnetic. It is unstable at $\beta = 0$ and is gradually stabilized with increasing β, with the consequent increase in the Shafranov shift and decrease in the amount of "bad" curvature. At this radius, the simplest ideal MHD

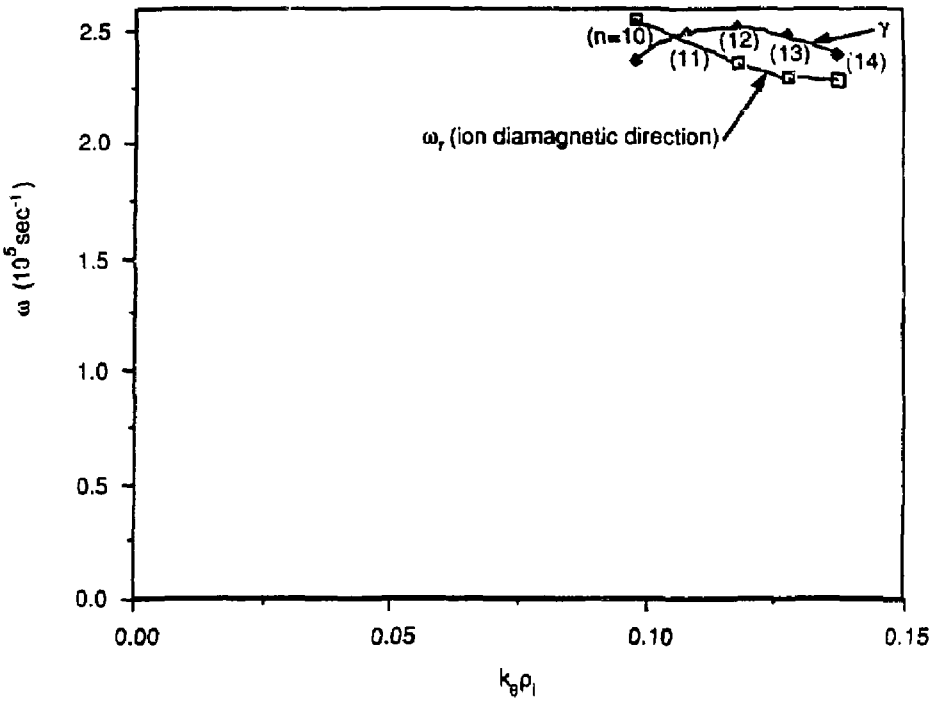

FIG. 9. Dependence of the growth rate and real frequency on n or $k_\theta \rho_i$ for the ω_{*pi} root without hot alpha particles for r = 11 cm, with β twice the BALDUR value, local β = 16.1%.

ballooning mode is stable for all β values, but in cases where it is unstable, the trapped-electron-η_i mode is normally unstable throughout the first stability region. The effect of hot alpha particles on this root is moderately stabilizing. It is unstable at the BALDUR calculated β values with or without alphas, unlike the ω_{*pi} or ω_A roots. In fact, it is the only one of the three modes that is predicted to be unstable and contribute to the quasilinear transport for the BPX case predicted by the BALDUR calculation.

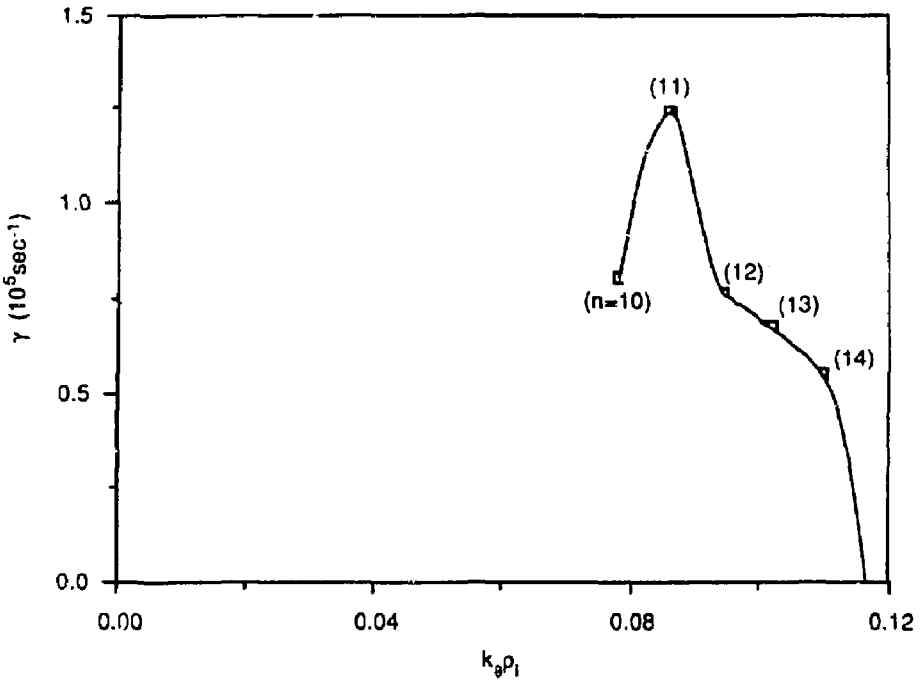

FIG. 10. Linear growth rate as a function of n or $k_\theta\rho_i$ for the ω_A root with hot alpha particles for $r = 15$ cm, with β twice the BALDUR value, local $\beta = 15.1\%$.

The corresponding real frequencies for the trapped-electron-η_i mode versus $\beta \propto n_j$ are shown in Fig. 8. They are relatively insensitive to variation in β. The effect of alpha particles on ω_r is quite small for this root.

2.3. Toroidal mode number dependence

The dependence of the growth rate and real frequency on n or $k_\theta\rho_i$ for the ω_{*pi} root without alpha particles is shown in Fig. 9. Here, $\beta(r)$ has been doubled from the BALDUR values to make the mode unstable, and $r = 11$ cm has been chosen to maximize the growth rate. The growth rate curve is fairly broad around the maximum at $n = 12$ or $k_\theta\rho_i = 0.12$.

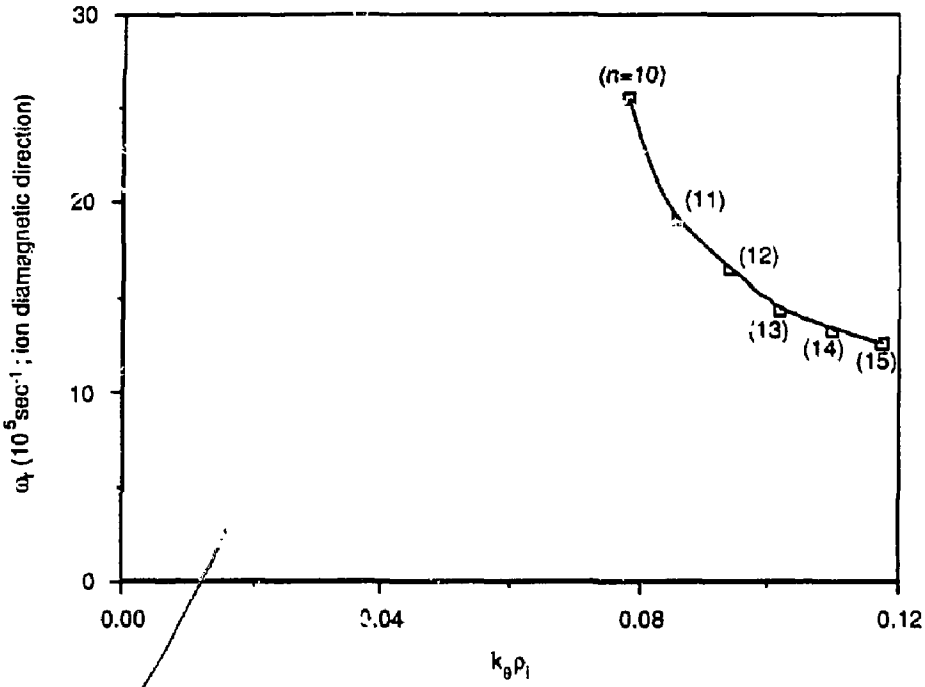

FIG. 11. Real frequencies corresponding to Fig. 10.

The corresponding dependences for the growth rate and real frequency of the ω_A root with alpha particles are shown in Figs. 10 and 11, respectively. For the same reasons, $\beta(r)$ has been doubled from the BALDUR values and $r = 15$ cm has been chosen. In Fig. 10, γ is seen to have a somewhat narrow maximum at $n = 11$ or $k_\theta\rho_i = 0.086$.

The trapped-electron-η_i mode has no maximum in r for the growth rate. At the original BALDUR $\beta(r)$ values without alpha particles, γ peaks for $n = 120$ or $k_\theta\rho_i = 0.34$ at $r = 41$ cm in the collisionless, electrostatic limit, and at $n = 375$ or $k_\theta\rho_i = 0.48$ at $r = 75$ cm in a fully electromagnetic but collisionless calculation.

2.4. Quasilinear transport

The linear eigenfrequency-eigenfunction calculation employed here also produces the quasilinear particle flux Γ_j and the total heat flux (including any convective portion) Q_j for each species j $(= e, i, \alpha)$. These fluxes are proportional to the square of the saturation level ϕ_0 for the perturbed electrostatic potential for the mode. This saturation level is not determined by the present linear and quasilinear calculation, but must be determined by some additional criterion. In the present work, the so-called "mixing length" saturation level is assumed, where $|e|\phi_0/T_e = C/\langle k_\perp \rangle r_p$, where C is a dimensionless constant of order unity, $\langle k_\perp \rangle$ is the average over the absolute squared eigenfunction of $k_\perp \equiv (k_\vartheta^2 + k_r^2)^{1/2}$, and $r_p \equiv -(d \ln p/dr)^{-1}$ is the total pressure gradient scale length. Also, $D_j^{\rm eff} \equiv -\Gamma_j/(dn_j/dr)$ is the effective particle diffusion coefficient and $\chi_j^{\rm eff} \equiv -Q_j/[n_j(dT_j/dr)]$ is the effective energy diffusion coefficient (thermal conductivity) for species j. In the present results, C is chosen such that $\chi_{\rm max}^{\rm eff} = 1 \times 10^4$ cm^2 sec^{-1}, where $\chi_{\rm max}^{\rm eff}$ is the maximum of $|\chi_e^{\rm eff}|$, $|\chi_i^{\rm eff}|$, and $|\chi_\alpha^{\rm eff}|$, so that the total thermal transport will be in a typical experimental range for present day tokamak experiments.

TABLE I. QUASILINEAR TRANSPORT FOR THE TRAPPED-ELECTRON-η_i MODE FOR THE BPX CASE

j	$D_j^{\rm eff}$(cm^2 sec^{-1})	Γ_j(cm^{-2} sec^{-1})	$\chi_j^{\rm eff}$(cm^2 sec^{-1})	Q_j(keV cm^{-2} sec^{-1})
e	-1.8×10^3	-5.0×10^{15}	-8.1×10^1	-7.8×10^{15}
i	-1.8×10^3	-5.0×10^{15}	$+1.0 \times 10^4$	$+9.4 \times 10^{17}$
α	$+6.9 \times 10^2$	$+2.3 \times 10^{13}$	$+1.1 \times 10^2$	$+2.9 \times 10^{15}$

Results are shown in Table I for the trapped-electron-η_i mode at $r = 39$ cm for $n = 114$ or $k_\vartheta \rho_i = 0.34$ at the BALDUR calculated β value (local $\beta = 3.93\%$), with $\eta_i = 3.77$ and $\eta_e = 3.83$. The normalization just described requires in this case that $|e|\phi_0/T_e = 0.18/\langle k_\perp \rangle r_p$. Among the $D_j^{\rm eff}$'s and the $\chi_j^{\rm eff}$'s, the dominant transport coefficient is $\chi_i^{\rm eff}$, as is typical for the η_i mode. The background electron and ion density profiles are very flat, so a slight inward particle flux occurs for them, driven by their normal temperature gradients. However, the

hot alpha particles, which have a very steep normal density profile, have an outward particle flux. In this case, $D_\alpha^{\rm eff}/\chi_i^{\rm eff} \simeq 0.07$, whereas in the previous cases in Ref. [3] for this mode, this ratio was several orders of magnitude smaller. Thus, in the present case, the trapped-electron-η_i mode can cause nonnegligible transport of the hot alpha particles, whereas in the previous cases in Ref. [3] this transport was insignificant. This sort of ratio is then highly case-dependent.

TABLE II. QUASILINEAR TRANSPORT FOR THE ω_{*pi} ROOT (THE MHD BALLOONING MODE) FOR THE BPX CASE

j	$D_j^{\rm eff}$(cm^2 sec^{-1})	Γ_j(cm^{-2} sec^{-1})	$\chi_j^{\rm eff}$(cm^2 sec^{-1})	Q_j(keV cm^{-2} sec^{-1})
e	-1.5×10^4	-1.4×10^{16}	$+6.2 \times 10^3$	$+1.9 \times 10^{18}$
i	-2.4×10^4	-1.6×10^{16}	$+1.0 \times 10^4$	$+2.7 \times 10^{18}$
α	$+3.3 \times 10^3$	$+5.5 \times 10^{14}$	$+2.5 \times 10^3$	$+3.8 \times 10^{17}$

For this case, the results for the ω_{*pi} root (the MHD ballooning mode) at twice the BALDUR β value (local $\beta = 16.1\%$), for $r = 11$ cm and $n = 12$, with $\eta_i = 26.8$ and $\eta_e = 19.5$, are given in Table II. For this root, the normalization discussed previously requires that $|e|\phi_0/T_e = 0.19/\langle k_\perp \rangle r_p$. Note that, for this root, $\chi_i^{\rm eff}$ and $\chi_e^{\rm eff}$ are roughly comparable, while $\chi_\alpha^{\rm eff}$ is several times smaller. A similar situation obtains for the $D_j^{\rm eff}$'s, except that the background electron and ion fluxes are inward, due to their nearly flat density profile, while that of the alphas is outward, due to their steep density profile.

TABLE III. QUASILINEAR TRANSPORT FOR THE ω_A ROOT (THE TAE OR "GAP" MODE) FOR THE BPX CASE

j	$D_j^{\rm eff}$(cm^2 sec^{-1})	Γ_j(cm^{-2} sec^{-1})	$\chi_j^{\rm eff}$(cm^2 sec^{-1})	Q_j(keV cm^{-2} sec^{-1})
e	-7.5×10^3	-1.0×10^{16}	-2.4×10^2	-6.0×10^{16}
i	-1.1×10^4	-1.2×10^{16}	-6.8×10^2	-1.6×10^{17}
α	$+4.0 \times 10^3$	$+6.3 \times 10^{14}$	$+1.0 \times 10^4$	$+1.4 \times 10^{18}$

The results for the ω_A root (the TAE or "gap" mode) at twice the BALDUR β value (local $\beta = 15.1\%$), for $r = 15$ cm and $n = 11$, with $\eta_i = 14.6$ and $\eta_e = 12.0$, are given in

Table III. For the ω_A root, $\chi_\alpha^{\rm eff}$ is largest and gives outward energy transport, while $\chi_i^{\rm eff}$ and $\chi_e^{\rm eff}$ are many times smaller, giving slight inward transport. Also, $D_\alpha^{\rm eff}$, $D_i^{\rm eff}$, and $D_e^{\rm eff}$ are all comparable in magnitude. Note though that the alpha particle transport is outward while the background electron and ion particle transport is inward, again due to the very steep alpha density profile and the very flat electron and ion density profiles.

2.5. Higher-order radial corrections

The preceding results have all been obtained at lowest order in the so-called "ballooning hierarchy", where the calculations are radially local to any chosen magnetic surface, yielding a lowest order eigenfrequency $\omega^{(0)}(r)$. At higher order in this hierarchy[12], in cases where the growth rate has a local maximum at some magnetic surface with $r = r_0$, it is possible to obtain a global eigenfrequency consisting of $\omega^{(0)}(r_0)$ plus the so-called "1/n" correction $\delta\omega$, where $\delta\omega = [2n(d\varrho/dr)]^{-1}[(\partial^2\omega^{(0)}/\partial r^2)(\partial^2\omega^{(0)}/\partial\theta_0^2)]^{1/2}$. Here, all of the derivatives are to be evaluated at $r = r_0$ and $\theta_0 = 0$, where θ_0 is the so-called "ballooning parameter", which is defined in Refs. [1], [2], and [12]. The value $\theta_0 = 0$ usually maximizes the lowest order growth rate in the case of an up-down symmetric MHD equilibrium, such as the one employed in the present BPX case.

For the ω_{epi} root considered in Section 2.1 with $n = 12$ for β double the BALDUR value, $r_0 = 11$ cm and $\omega^{(0)}(r_0) = (-2.166 + 0.735i) \times 10^5$ sec^{-1}. Evaluating the necessary derivatives numerically, it is found that $\delta\omega = (0.309 - 0.335i) \times 10^5$ sec^{-1}. Thus, the effect of including this "1/n" correction term is roughly to cut the linear growth rate at $r = r_0$ in half. The ω_{epi} root is, however, still unstable in this situation.

The same procedure has been carried out for the ω_A root with $n = 11$ for β double the BALDUR value, where $r_0 = 15$ cm and $\omega^{(0)}(r_0) = (-19.15 + 1.24i) \times 10^5$ sec^{-1}. For this root, evaluating the derivatives numerically yields $\delta\omega = (3.79 - 4.68i) \times 10^5$ sec^{-1}, so that this root would actually become damped at this order. However, $\delta\omega$ is sufficiently large compared to γ that the underlying expansion in powers of $n^{-1/2}$ is not properly convergent. In fact, a more

general formulation, which has not been derived for the fully kinetic case[12], appears to be needed here. In any event, the implication is that this instability will be severely weakened by higher order effects that have not been included in the results presented in the preceding sections Never the less, it seems worthwhile to present the results here for the ω_A root on the same basis as those for the ω_{*pi} root and the trapped-electron-η_i mode.

The trapped-electron-η_i mode presents a related problem. As seen in Section 2.1, there is no radial local maximum for the growth rate for this root. So again, the formulation for $\delta\omega$ given previously does not apply. However, the value of n involved with this root, $n = 114$ instead of 11 or 12, suggests that $\delta\omega$ should be considerably smaller for the trapped-electron-η_i mode than for the ω_{*pi} root or the ω_A root.

3. TFTR CASE

Results are presented in this section for the ω_{*pi} root (the MHD ballooning mode) only for the TFTR case mentioned in Section 1. The equilibrium profiles for $n_j(r)$, $T_j(r)$, and $q(r)$ are taken from a TRANSP transport code run[11] for an extrapolation of a particular TFTR deuterium supershot to an equal deuterium-tritium mixture, giving $Q \simeq 0.5$. The corresponding fixed-boundary MHD equilibrium is computed numerically. The parameters are: $R_0 = 2.5$ m, $B_0 = 5.2$ T, $I_p = 2.1$ MA, $a = 0.85$ m, elongation at boundary = 1.0, triangularity at boundary = 0, $q(0) = 0.92$, $q(a) = 3.58$, $T_e(0) = 9.73$ keV, $T_i(0) = 28.92$ keV, $n_e(0) = 1.092 \times 10^{14}$ cm^{-3}, $\beta(0) = 7.29\%$ without hot alpha particles, and $n_\alpha(0)/n_e(0) = 0.0056$. For this case, the electron density profile and the ion and electron temperature profiles are all comparably localized, while the hot alpha particle density profile is substantially more localized. Results will be presented only for a single magnetic surface at $r = 14.9$ cm, which is the magnetic surface where the growth rate from the simplest ideal MHD ballooning mode equation is a maximum. Here, the local parameters are: $T_e = 8.99$ keV, $T_i = 24.80$ keV, $n_e = 9.17 \times 10^{13}$ cm^{-3}, $q = 0.966$, $\beta = 4.62\%$ without alpha particles, $\beta = 5.11\%$ with alpha particles, $n_\alpha/n_e = 0.0048$, $r_{n\alpha}/r_{ne} = 0.498$, $\eta_e = 0.455$, and $\eta_i = 1.09$

without alpha particles. Again, the hot alpha particle equilibrium distribution function is taken to be a "slowing down" distribution.

As in the BPX case, β will be varied artificially for the TFTR case by multiplying all the $n_j(r)$ by a constant at fixed $T_j(r)$ and B_0, and then recomputing the MHD equilibrium numerically. Also, the hot alpha particle contribution will be turned off for comparison by replacing the alphas by background ions, at fixed $n_e(r)$, with n_i and r_{ni}/r_{ne} being adjusted to preserve the conditions of equilibrium charge neutrality and its radial derivative on the chosen magnetic surface.

Results for the linear growth rate versus β for the ω_{*pi} root or MHD ballooning mode are shown in Fig. 12 for this TFTR case. Here, $n = 10$ or $k_\theta \rho_i = 0.34$ or $k_\theta \rho_\alpha = 1.2$, the values which maximize the linear growth rate on this magnetic surface at the TRANSP calculated β value. Also, the growth rate from the simplest ideal MHD ballooning mode equation, without diamagnetic or FLR effects and without alpha particles, is shown for reference. The addition of all of the kinetic effects other than the hot alpha particles to the simplest ideal MHD ballooning mode is generally to reduce the growth rate in the unstable region, but also to lower the kinetic critical β, $\beta_c^{\rm kin} \simeq 2.15\%$, to be well below the ideal MHD critical β, $\beta_c^{\rm MHD} \simeq 3.5\%$. For $\beta \gtrsim 5\%$, the usual nonresonant interchange instability mechanism accounts for the growth rate, but for $\beta < 5\%$, the kinetic dissipation from mode-particle resonances can dominate the growth rate. This is the same mechanism that destabilizes the resistive MHD ballooning mode, adding a "tail" to the ideal MHD growth rate curve for $\beta < \beta_c^{\rm MHD}$. However, in this case, the resonant dissipation rather than the collisional resistive dissipation is the primary source of the instability. Then, with the addition of the hot alpha particles, the critical β value is further reduced, to $\beta_c^a \simeq 0.6\%$. There is a "crossover" β value $\simeq 5.3\%$, above which the effect of the hot alphas is stabilizing, apparently because their presence interferes with the nonresonant interchange mechanism. However,

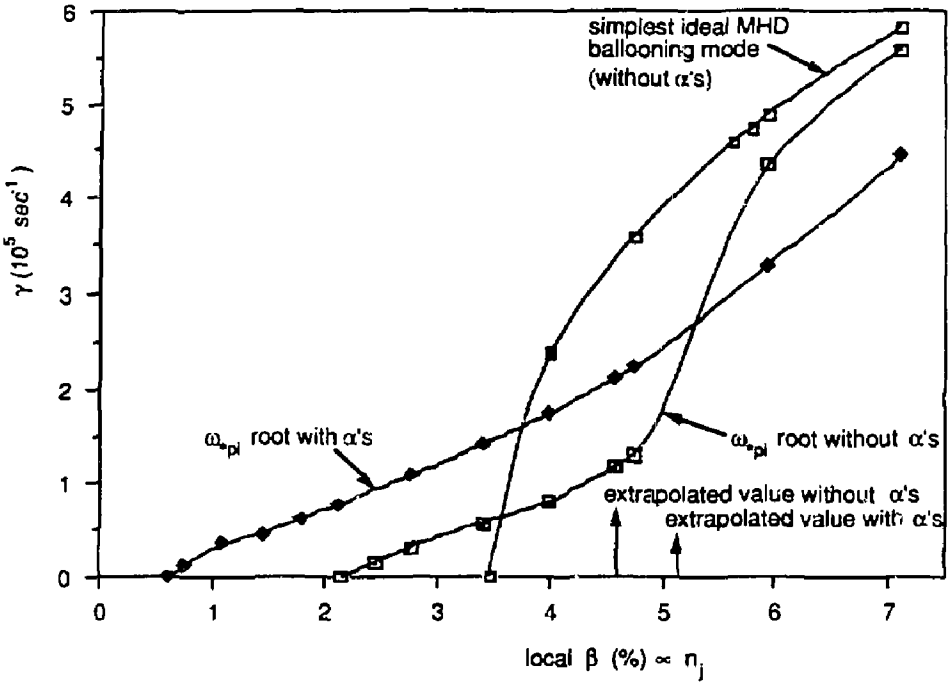

FIG. 12. Dependence of the linear growth rate on $\beta \propto n_j$ for the ω_{*pi} root in the TFTR $Q = 0.5$ case, as in Fig. 3, with and without hot alpha particles. Here, $r = 14.9$ cm, $n = 10$, $k_\theta \rho_i = 0.34$, and $k_\theta \rho_\alpha = 1.2$.

for $\beta < 5.3\%$, the alphas are destabilizing because their mode-particle resonances provide substantial additional dissipation to reinforce that from the background species.

The corresponding real frequencies are shown in Fig. 13, with and without the hot alpha particles. (The real frequency for the simplest ideal MHD ballooning mode is just zero.) The kinetic real frequencies are of the same order as ω_{*pi} and $\bar{\omega}_{d\alpha}$, the average hot alpha magnetic drift frequency, and are between $\bar{\omega}_{b\alpha}$, the average trapped alpha bounce frequency, and $\bar{\omega}_{t\alpha} \simeq 24 \times 10^5$ sec^{-1}, the average untrapped alpha transit frequency. They are substantially below $\omega_A \simeq 30 \times 10^5$ sec^{-1}.

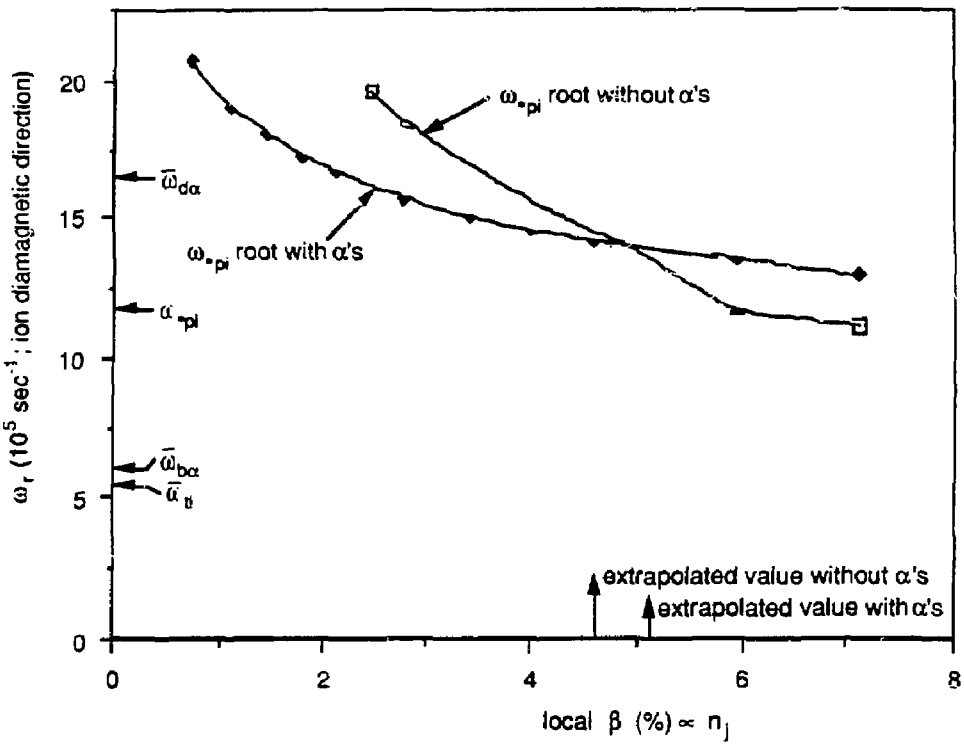

FIG. 13. Real frequencies corresponding to Fig. 12.

The quasilinear transport results for this ω_{*pi} root at $\beta = 4.62\%$ with $n = 10$ are given in Table IV. For this case, all of the particle and energy fluxes are outward, with $D_\alpha^{\rm eff} \gtrsim D_e^{\rm eff} \simeq D_i^{\rm eff}$ and $\chi_e^{\rm eff} \gtrsim \chi_i^{\rm eff} \gtrsim \chi_\alpha^{\rm eff}$.

TABLE IV. QUASILINEAR TRANSPORT FOR THE ω_{*pi} ROOT (THE MHD BALLOONING MODE) FOR THE TFTR CASE

j	$D_j^{\rm eff}$(cm^2 sec^{-1})	Γ_j(cm^{-2} sec^{-1})	$\chi_j^{\rm eff}$(cm^2 sec^{-1})	Q_j(keV cm^{-2} sec^{-1})
e	$+2.1 \times 10^3$	$+3.7 \times 10^{15}$	$+1.0 \times 10^4$	$+7.1 \times 10^{16}$
i	$+2.1 \times 10^3$	$+3.6 \times 10^{15}$	$+7.1 \times 10^3$	$+3.3 \times 10^{17}$
α	$+3.3 \times 10^3$	$+5.7 \times 10^{13}$	$+3.4 \times 10^3$	$+4.5 \times 10^{16}$

4. CONCLUSIONS

One of the major points of the present study is to compare the properties of three separate types of high-n instabilities for the same BPX case from the same comprehensive kinetic calculation. These are the MHD ballooning mode, also called the ω_{*pi} root, the toroidicity-induced Alfvén eigenmode or "gap" mode, also called the ω_A root, and the toroidal drift mode, also called the trapped-electron-η_i mode. Radially, the linear growth rate curves for both the ω_{*pi} root and the ω_A root have maxima inside the $q = 1$ surface, where $|dp/dr|$ is the largest. The growth rate curve for the trapped-electron-η_i mode, on the other hand, rises strongly out to the plasma boundary, with no local maximum, for this case with a very flat background density profile. The β dependence of the three types of growth rates is investigated by scaling all of the density profiles $n_j(r)$ at fixed $T_j(r)$ and B_0. Varying β this way, the ω_{*pi} root and the ω_A root are unstable only above a critical β value which is slightly below the simplest ideal MHD critical β, while the trapped-electron-η_i mode is unstable even at $\beta = 0$, and has a growth rate that decreases gradually with increasing β. The effect of adding hot alpha particles, by replacing background ions at fixed $n_e(r)$, is to decrease the growth rate for the ω_{*pi} root and the trapped-electron-η_i mode, whereas the alpha particles increase the growth rate for the ω_A root, and in fact are necessary for it to be unstable at all, for this case. At the BALDUR calculated β values, only the trapped-electron-η_i mode is unstable, since the critical β values for the ω_{*pi} root and the ω_A root, including the effects of hot alpha particles, are above these predicted values. Varying the toroidal mode number n, or equivalently $k_\theta \rho_i \propto n$, it is found that the growth rates are maximized for $n \simeq 11$–12 or $k_\theta \rho_i \simeq 0.1$ for the ω_{*pi} root and the ω_A root, while that for the trapped-electron-η_i mode peaks at $k_\theta \rho_i \simeq 0.3$–$0.5$, with an n value that depends on radius.

The quasilinear particle and energy fluxes and effective transport coefficients for each species have also been calculated for each of the three roots in situations where they are unstable. Though there are different results for the three types of instabilities that have been described in Section 2.4, they can all lead to anomalous particle transport for the hot

alphas that is roughly of the same order as that of the background species. For the trapped-electron-η_i mode, this case is different from those previously described in Ref. [3], where the hot alpha particle transport from this mode was several orders of magnitude smaller than that for the background species.

The preceding results have all been calculated at lowest order in the so-called "ballooning hierarchy", where the eigenfrequency calculation is local to each chosen flux surface. At higher order in this hierarchy, the so-called "$1/n$" correction term has been calculated for the ω_{*pi} root and the ω_A root at the surfaces where their linear growth rates have their respective radial maxima. The results indicate that the growth rate for the ω_{*pi} root is reduced by about a factor of two, while the ω_A root is likely to be completely stabilized.

Another case has been considered here which models TFTR in a deuterium-tritium mode of operation with $Q \simeq 0.5$. For the ω_{*pi} root in this TFTR case, unlike the BPX case, the overall result of the kinetic effects omitted from the usual simplest ideal MHD ballooning mode analysis, and of the hot alpha particles, is to drastically lower the critical β value for instability, from a local $\beta \simeq 3.5\%$ down to local $\beta \simeq 0.6\%$. This same trend was seen in one of the cases considered in Ref. [3], but not in the other, and not in the BPX case considered here. This sort of drastic lowering of the critical β for the MHD ballooning mode, then, seems to be very case-dependent. Again for this TFTR case, the quasilinear transport has been calculated for the ω_{*pi} root, and it is seen that the particle transport for the hot alphas is roughly of the same order as that for the background particles.

ACKNOWLEDGMENTS

The author would like to thank Dr. G. Bateman for providing the transport code results for the BPX case, and Drs. D. Mikkelsen and R. Budny for providing those for the TFTR case. He would also like to thank Drs. D. Sigmar, L. Chen, W. M. Tang, and S. J. Zweben for informative discussions, and he is grateful to Dr. Tang for reading and suggesting improvements in a draft of this paper.

This work was supported by United States Department of Energy Contract No. DE-AC02-76-CHO-3073.

REFERENCES

[1] REWOLDT, G., TANG, W.M., CHANCE, M.S., Phys. Fluids **25** (1982) 480.

[2] REWOLDT, G., TANG, W.M., HASTIE, R.J., Phys. Fluids **30** (1987) 807.

[3] REWOLDT, G., Phys. Fluids **31** (1988) 3727.

[4] CHENG, C.Z., CHANCE, M.S., Phys. Fluids **29** (1986) 3695.

[5] CHENG, C.Z., CHEN, L., CHANCE, M.S., Ann. Phys. (NY) **161** (1985) 21.

[6] CHENG, C.Z., Alpha Particle Destabilization of the Toroidicity-Induced Alfven Eigenmodes, Rep. PPPL-2717, Princeton Plasma Physics Laboratory, Princeton, NJ (1990).

[7] WONG, K. L., FONCK, R. J., PAUL, S. F., *et al.*, Phys. Rev. Lett. **66** (1991) 1874.

[8] REWOLDT, G., TANG, W.M., Phys Fluids B **2** (1990) 318

[9] GOLDSTON, R.J., BATEMAN, G., BELL, M.G., *et al.*, Bull. Am. Phys. Soc. **35** (1990) 1920.

[10] SINGER, C.E., POST, D.E., MIKKELSEN, D.R., *et al.*, Comp. Phys. Comm. **49** (1988) 275.

[11] MIKKELSEN, D.R., BUDNY, R.V., CHENG, C.Z., *et al.*, Bull. Am. Phys. Soc. **35** (1990) 2087.

[12] FRIEMAN, E.A., REWOLDT, G., TANG, W.M., GLASSER, A.H., Phys. Fluids **23** (1980) 1750.

[13] BETTI, R., FRIEDBERG, J.P., Ellipticity induced Alfvén eigenmodes, Rep. PFC/JA-91-1, Massachusetts Institute of Technology Plasma Fusion Center, Cambridge, MA (1991); Phys. Fluids, in press.